TU Delft

Delft University of Technology

Document Version
Final published version

Licence
CC BY

Citation (APA)
Woigk, W., Patranabish, S., Hao, J., Rion, J., van Vuure, A. W., Dransfeld, C., Hegemann, D., Fuentes, C. A., & Masania, K. (2026). Atmospheric pressure plasma enhances the mechanical properties of natural fibre-reinforced polyoxymethylene thermoplastic composites. *Composites Part A: Applied Science and Manufacturing*, *211*, Article 110202. https://doi.org/10.1016/j.compositesa.2026.110202

Important note
To cite this publication, please use the final published version (if applicable).
Please check the document version above.

Copyright
In case the licence states “Dutch Copyright Act (Article 25fa)”, this publication was made available Green Open Access via the TU Delft Institutional Repository pursuant to Dutch Copyright Act (Article 25fa, the Taverne amendment). This provision does not affect copyright ownership.
Unless copyright is transferred by contract or statute, it remains with the copyright holder.

Sharing and reuse
Other than for strictly personal use, it is not permitted to download, forward or distribute the text or part of it, without the consent of the author(s) and/or copyright holder(s), unless the work is under an open content license such as Creative Commons.

Takedown policy
Please contact us and provide details if you believe this document breaches copyrights.
We will remove access to the work immediately and investigate your claim.

This work is downloaded from Delft University of Technology.

Composites: Part A 211 (2026) 110202

Contents lists available at ScienceDirect

Composites Part A

journal homepage: www.elsevier.com/locate/compositesa

Atmospheric pressure plasma enhances the mechanical properties of natural fibre-reinforced polyoxymethylene thermoplastic composites

W. Woigk [a], S. Patranabish [b], J. Hao [c,d,e], J. Rion [f], A.W. van Vuure [c], C. Dransfeld [a,h], D. Hegemann [f], C.A. Fuentes [c,g], K. Masania [a,b,*]

[a] Institute of Polymer Engineering, FHNW University of Applied Sciences and Arts Northwestern Switzerland, CH-5210 Windisch, Switzerland
[b] Shaping Matter Lab, Faculty of Aerospace Engineering, Delft University of Technology, Kluyverweg 1, 2629 HS Delft, the Netherlands
[c] Department of Materials Engineering, KU Leuven, B-3001 Heverlee, Belgium
[d] Department of Mechanics of Materials and Constructions, Vrije Universiteit Brussel, Brussels, Belgium
[e] Bcomp Ltd., CH-1700 Fribourg, Switzerland
[f] Empa, Swiss Federal Laboratories for Materials Science and Technology, CH-9014 St. Gallen, Switzerland
[g] Structural Composites Unit, Luxembourg Institute of Science and Technology, L-4940 Hautcharage, Luxembourg
[h] Aerospace Manufacturing Technologies, Faculty of Aerospace Engineering, Delft University of Technology, Kluyverweg 1, 2629 HS Delft, the Netherlands

ARTICLE INFO

Keywords:
Naturalfibre composites
Thermoplastic matrices
Plasma treatment
Atmospheric pressure plasma
Interfaces

ABSTRACT

The development of sustainable and high-performance composite materials necessitates effective strategies to improve compatibility between natural fibres (NFs) and circular thermoplastic matrices. We report atmospheric pressure (AP) plasma treatment as a scalable, interface-engineered approach to enhance the mechanical performance of unidirectional flax fibre (FF)-reinforced polyoxymethylene copolymer (coPOM) composites. FF fabrics were treated using diffuse coplanar surface barrier discharge plasma and processed into high fibre volume fraction (FVF ~ 61%) composites via film stacking. Post-treatment surface analysis revealed removal of waxy species and increased oxygen-containing functional groups, reflected by an increased O/C ratio (from 0.48 to 0.74) and elevated total surface energy (from 29.4 to 41.8 mJ/m^2). The wetting improved significantly, with spreading coefficient changing from − 3.9 mJ/m^2 to positive values. At the coupon level, transverse tensile modulus and strength increased by ~ 67 % and ~ 23 %, and transverse compressive modulus and strength by ~ 46 % and ~ 43 %, respectively. Shear strength (~ 23%) and in-plane shear moduli (~ 31 %) were also enhanced. In contrast, longitudinal tensile strength decreased by ~ 12% despite a 12% increase in longitudinal modulus, while failure-envelope analysis indicated an expanded inter-fibre failure domain. Together, the results highlight AP plasma treatment as a roll-to-roll-compatible route to significantly improve off-axis mechanical performance of NF/thermoplastic composites.

1. Introduction

In today's growing environmental awareness and the necessity to reduce greenhouse gas emissions have a strong influence on the material selection and part engineering for industrial and structural applications. Reducing the consumption of fossil-based resources is closely linked to lightweight design, which has driven the widespread use of fibre-reinforced plastics based on carbon fibres, glass fibres, and aramid fibres owing to their high property-to-weight ratio.[1,2] To reduce the environmental impact further, an increased demand for materials that are recyclable and bio-based or biodegradable can be observed.[3,4] Natural fibres (NFs) exhibit such desired attributes and have therefore attracted growing interest, particularly in the fields of aircraft interiors, automotive, sports, building and construction. [5,6] They offer clear advantages including lower processing costs, lower energy consumption, and the likelihood of carbon–neutral processing due to CO_2 consumption/capture during their natural growth. [7]

Among NFs, flax, hemp, jute, kenaf and coir fibres have been widely studied. Flax fibres (FF) have shown high potential as reinforcing fibres due to their low density (1.50 g/cm^3) and high specific mechanical properties, which can challenge those of common synthetic fibre-reinforced composites. [8] Young's modulus values up to 80 GPa have

* Corresponding author..
E-mail address: k.masania@tudelft.nl (K. Masania).

https://doi.org/10.1016/j.compositesa.2026.110202
Received 1 April 2026; Received in revised form 4 August 2026; Accepted 15 August 2026
Available online 16 August 2026
1359-835X/© 2026 The Author(s). Published by Elsevier Ltd. This is an open access article under the CC BY license (http://creativecommons.org/licenses/by/4.0/).

been reported for elementary FF, [9] while excellent multiscale vibration damping (up to ~ 65.4%) and impact energy absorption characteristics have also been demonstrated. [10,11] In addition, FF provide a high potential to capture CO_2 during growth (~ 1.3–1.4 kg CO_2/kg fibre) and require comparatively low production energy. FF consists of approx. 71% cellulose, 20% hemicellulose, 2% pectin, 2% lignin, and 2% wax, the latter being mainly at the surface of the fibres. [12] Since the outer wax layer hampers adhesion in a composite material, a boiling process is typically applied to remove the waxy substances. A common cleaning procedure with boiling acetone (around 45 min), however, shows a limited cleaning effect. [13,14] Therefore, often a multi-step boiling process is applied, such as pre-boiling with acetone followed by an alkali treatment with NaOH solution, followed by rinsing and drying. [12,14] Whilst, this process removes waxy substances and lignin portions from FF, [14,15] it is time- and energy-intense and results in severe weight loss of the flax material (12–13%), strongly affecting its morphological and mechanical properties. [16].

In the context of matrix materials, thermoplastics are of particular interest because they are more sustainable, circular, allow for low-cost processing, and typically provide high toughness. [17] However, their stiffness and strength are often inherently lower than those of thermoset matrices, and compatibility with NFs is frequently limited. [18] In many NF/thermoplastic composites, the fibre/matrix interface is dominated by physical and mechanical interactions, which can restrict stress transfer and mechanical performance. A particularly interesting thermoplastic polymer is polyoxymethylene (POM), which is often used for semi-structural parts such as gear wheels and pulleys because of its high strength, durability, and excellent impact performance. Moreover, owing to its comparatively low melting temperature, POM copolymer (coPOM), typically produced by copolymerising trioxane with small amounts of cyclic ether/acetal comonomers, has recently been considered as a matrix material for NF composites. [19] It was shown previously that impregnation of FF fabrics with coPOM can be sufficiently high to allow for composites that demonstrate mechanical properties similar to FF/epoxy counterparts. Despite these good mechanical properties, limitations in the impregnation process can still be identified from microscopy images, [13] motivating further work to dewax and increase the surface free energy of the fibre for better impregnation and adhesion.

A major challenge is to improve the properties at the interface between NFs and thermoplastic matrices. [19–21] While the bulk of NFs is inherently hydrophilic due to the presence of hydroxyl and other polar functional groups, their raw outer surface features a waxy coating that renders them hydrophobic. When combined with hydrophobic thermoplastic matrices, this surface mismatch leads to poor interfacial interactions and weak adhesion, potentially reducing the NF's effectiveness as reinforcing fibres. Interestingly, these polar groups of NF can also enhance the adhesion and interfacial properties when used with a compatible matrix containing reactive or polar functionalities. Therefore, the polar nature of NFs is not necessarily disadvantageous when matched with the proper matrix material and surface engineering of the fibres.

Apart from polarity, other factors such as surface heterogeneity, variability of surface properties, and composition of the fibre itself contribute to the interfacial behaviour. Alongside the main constituents, waxy substances can also be present on the fibre surface, [19] which can affect wetting, impregnation, as well as interfacial load transfer. Therefore, it is crucial to engineer NF composites with respect to the fibre, the matrix, and their compatibility, which requires analysis and improvement of the fibre/matrix interfaces. To improve the compatibility between fibre and matrix for achieving effective stress transfer, two routes are commonly pursued – utilisation of grafted polymers and fibre surface treatments. While the first requires chemical modifications, the latter is aimed to enhance the wetting, interfacial adhesion, and ultimately the mechanical performance of the composite.

In unidirectional composites, transverse and in-plane shear properties are dominated by the physical performance of the matrix and the fibre–matrix interface. Matrix modifications through grafting or copolymerisation have been shown to enhance the composite's mechanical properties. For example, improvement in mechanical properties has been reported in both transverse and shear loading in maleic anhydride-grafted polypropylene (MAPP) composites, [22] and even in the fibre-dominated longitudinal direction in cellulose propionate (CP), where fibre and matrix have similar compositions. [23] MAPP has been studied for more than one decade and has proven to be a standard solution to significantly enhance the interfacial strength of NF composites. [22] Fuentes et al. [24] studied matrix/substrate compatibility and showed that fibre/matrix adhesion can be realized through the formation of covalent bonds, similar to epoxy systems, resulting in very high interfacial properties. Alternatively, interfacial properties can be enhanced by functionalising and activating the fibre surface prior to composite processing/impregnation. Fibre surface treatments can generally be categorized into chemical and physical approaches. Chemical treatments such as alkali treatment, acetylation and benzoylation involve harsh chemicals which may not only be detrimental to the fibre itself but also have environmental implications after processing. [12] These also predominantly change the fibre morphology and chemical composition. [25] In contrast, physical methods can alter fibre surface chemistry through cleaning, removal of weakly attached waxy substances, and introduction of new functional groups. [26] Physical treatments such as plasma and corona treatments and electron beam irradiation, can clean the surface, remove waxy substances, and add functional groups to the fibre surface. [27,28].

Plasma is an ionized gas containing electrons, ions, neutral particles and excited species, and is approximately quasi-neutral in its bulk. [29] Depending on the gas environment, plasma can produce free radicals, introduce reactive groups, increase or decrease surface energy, and remove contaminating substances, although the stability of these induced surface modifications may vary. [25,30] Functional groups, which enable high affinity and compatibility to the matrix polymer, are grafted onto the fibre surface. [31] Sachs et al. [13] applied atmospheric pressure dielectric barrier discharge (APDBD) treatment in a roll-to-roll setup on FF. They found that plasma causes a combination of wax removal and formation of oxygen-containing groups. Seghini et al. [32] investigated oxygen and tetravinylsilane plasmas for FF composites with epoxy and vinylester matrices. Despite increased roughness, functional groups, and enhanced interfacial adhesion on single yarns, the composite mechanical properties were found to be reduced. Bozaci et al. [27] studied argon and air atmospheric plasma treatments on interfacial adhesion between FF and the matrix. They reported enhanced interfacial shear strength, changes in surface chemistry, and newly created functional groups, but also fibre damage and loss of fabric integrity depending on the plasma power. Sarikanat et al. [33] used argon and air atmospheric pressure plasma treatments to improve FF-reinforced unsaturated polyester composites and reported increases of ~ 34% in tensile strength, ~ 31% in flexural strength, ~ 39% in interlaminar shear strength (ILSS), ~ 35% in Mode I fracture toughness (GIC), and ~ 42% in Mode II fracture toughness (GIIC). Baltazar-y-Jimenez et al. [34] reported a significant decrease in the mechanical properties after an atmospheric air pressure plasma treatment on lignocellulosic fibres due to dehydration caused by the heat generated by the plasma and degradation of the fibre's microstructure. Despite the deterioration of the microstructure and mechanical properties, an enhanced interfacial shear strength was recorded due to the functionalisation, surface cleaning, and increased roughness. Marais et al. [28] combined autoclave and helium cold plasma treatments on flax non-wovens. They reported reduced water diffusivity and deposition of free radicals, where the radicals enabled covalent bonding with an unsaturated polyester matrix during curing while the cleaned surface facilitated adhesion. However, the increment in tensile properties were negligible, suggesting limited mechanical interlocking. Seki et al. [35] studied radio-frequency and low-frequency O_2 plasmas for jute/polyester composites and reported

increases in the tensile and flexural strength, with a more pronounced increase of around 129% in ILSS.

Despite the evidence for surface cleaning and functionalisation, further optimisation of plasma treatment is required. Compared with low pressure (LP) plasma, atmospheric pressure (AP) plasma avoids vacuum equipment and is more readily integrated into continuous, large-area processing, making it particularly attractive for industrial surface treatment. [36,37] At atmospheric pressure, the higher gas density and more frequent collisions typically confine the discharge to relatively thin plasma regions or micro discharges.[38] At LP, on the contrary, high energetic electrons drive the activation reactions such as excitation, dissociation and ionisation by multiple electron collisions in the plasma. Most of all, the use of oxygen (O_2) gas results in a highly reactive plasma due to relatively low activation energies. O_2 plasmas have thus been reported to yield strong etching conditions on FF and other NFs resulting in a reduction of their mechanical properties. [33,35,39] For this reason, carbon dioxide (CO_2) is used as reactive gas with a small admixture of argon (Ar) to support homogeneous plasma spreading over large areas, for controlled activation reactions at LP. [15] Petrov et al. [40] give a set of collision cross sections for excitation, dissociation and ionisation to compare O_2, N_2, and CO_2. At AP conditions, due to the lower electron temperature O_2 might be well suited together with a carrier gas that can also be N_2. Consequently, air represents an appropriate, low-cost gas for the plasma treatment of FF. [13,27,41].

We hypothesise that atmospheric-pressure (AP) plasma treatment using air (O_2 and N_2. species) can provide a controlled, cost-effective surface activation of FFs without inducing the severe degradation of mechanical properties typically caused by low-pressure (LP) plasma etching. The objective of this study is therefore to evaluate the effectiveness of LP and AP treatment for the surface activation of FFs. We aim to investigate whether the milder chemical reactions and lower electron temperatures at atmospheric pressure can successfully modify FF surfaces without causing the mechanical degradation typically seen with low-pressure oxygen etching.

We study the interfacial properties and mechanical performance of unidirectional FF-reinforced coPOM thermoplastic composites. Detailed analysis of surface chemistry and surface energy is presented to quantify plasma-induced modifications, followed by coupon-level composite material characterisation under tensile, compressive, and in-plane shear loading in both longitudinal and transverse sample configurations. The results demonstrate significant improvements in both matrix-dominated and interface-dominated properties, accompanied by changes in the failure behaviour and inter-fibre failure envelope. The study provides comprehensive engineering data for FF-reinforced coPOM composites, where coPOM has previously been shown to be a highly suitable thermoplastic matrix material. [19] Our findings also present an innovative and scalable approach towards advancing the NF thermoplastic composites as sustainable composites.

2. Materials & methods

2.1. Flax fibre (FF)

Raw FFs before wet spinning, and wet spun UD-woven FF fabrics (ampliTex® UD type 5009, abbr. ampUD) with an areal weight of 300 g/m^2 were provided by Bcomp Ltd. (Fribourg, Switzerland). The yarns have a nominal linear density of 105 tex and exhibit a twist level of 260 ± 40 turns per metre. NFs typically exhibit a low decomposition temperature in the range of about 170–190 °C, varying according to atmospheric conditions and the duration of exposure to elevated temperatures.[42] Therefore, the polymer melt temperature during manufacturing should not exceed the fibre's degradation temperature for prolonged times.

2.2. Polymers and matrix processing

Hostaform C 9021 XAP polyoxymethylene copolymer (coPOM) (Celanese, USA), with a melt flow index (MFI) of 11 g/10 min at 190 °C and 2.16 kg was used as the matrix material. Films with a width of 80 mm and a thickness of approximately 100 μm were produced using a Collin (Dr. Collin GmbH, Germany) Teach-Line extruder equipped with a slit die. The feedstock materials, in the form of pellets, were dried overnight and fed to the extrusion machine. The temperatures of the heating zones were gradually increased from 50 °C in the feeding zone up to 210 °C. Films were drawn from the extruder die through two rotating and water-cooled rollers and collected to a winding cylinder.

2.3. Plasma treatment

The plasma treatments were carried out using two different processes as shown in Fig. 1, characterised by the power and ambient conditions used for the process. Under low-pressure (LP) conditions, energetic ions and reactive radicals interact over larger sheath distances of ~ mm with high kinetic impact in the range 10–100 eV. Conversely, atmospheric-pressure (AP) surface discharge confines these active species to a thin layer < 0.1 mm directly adjacent to the fibre surface at lower energies of 1–3 eV which we hypothesise, should prevent structural cell-wall degradation.

At first, a low-pressure plasma was used for general investigation. For low pressure, a laboratory-built pilot-scale web coater was used, which allows for semi-continuous processing of FF fabrics up to a width of 650 mm.[43] The LP plasma treatments on FF fabrics were performed on a rotating drum (590 mm in diameter), which is connected to 13.56 MHz radio frequency (RF) excitation (capacitive coupling). LP plasma can be highly conformal, [44,45] and the FF fabrics were thus treated from one side in all cases. A gas shower with four inlet positions ensured homogeneous treatment over the electrode area of about 1 m^2. The treatment was performed in an CO_2/Ar atmosphere, 400:25 SCCM, at 700 and 1000 W of power, under 10 Pa of pressure. These parameters were selected as a stable and reproducible operating condition within the established operating window of the pilot-scale reactor.

The CO_2 and Ar flow rates of 400 and 25 sccm, respectively, were selected as a stable and reproducible operating condition within the established operating window of the pilot-scale reactor. This composition was not determined as a global optimum for maximum reactive-species concentration, and no plasma-phase diagnostic measurements were performed during these experiments. Instead, the effects of plasma power and exposure time were evaluated ex situ through residual-wax quantification and XPS analysis of the O/C ratio and surface functional-group distribution.

To facilitate industrial scalability, an atmospheric-pressure plasma process was also studied. The atmospheric-pressure plasma treatments were carried out using a Diffuse Coplanar Surface Barrier Discharge (DCSBD) device. [46] An embedded electrode structure within a ceramic tile creates micro discharges distributed above an area of approx. 200 x 80 mm^2 with plasma layer thickness of about 0.3 mm. During treatment, the flax fabric was guided directly through this plasma layer at a nominal stand-off distance of approximately 0.1–0.3 mm from the ceramic surface. The DCSBD was operated in ambient air under open atmosphere conditions and therefore no controlled gas-flow rate was imposed, and no external process gas was used. Plasma exposure times of 10 s, 30 s, and 5 min corresponding to a R2R speed of 0.5, 0.16, and 0.016 m/min, respectively, were selected. The DCSBD was operated at a nominal power of 350 W for the 30 s and 5 min treatments, and at 370 W for the continuous 10 s treatment. These correspond to nominal areal power densities of approximately 2.19 W/cm^2 and 2.31 W/cm^2, respectively. The AP plasma can only be directly applied to one side of the material, i.e. the side closely facing the plasma device. In the case of a porous medium such as a textile fabric, the immersion depth of the plasma is an important parameter affecting the homogeneity of the plasma treated

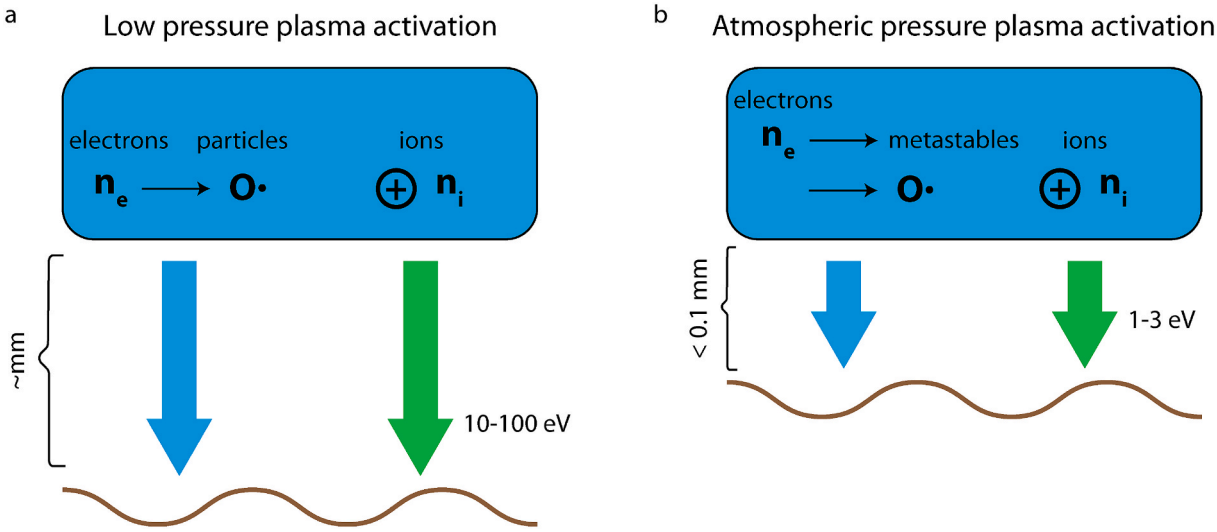


Fig. 1. To illustrate the physical differences and active species interaction zones between: **a** low-pressure (LP) capacitive coupling plasma and **b** atmospheric-pressure (AP) coplanar barrier discharge. Under LP conditions, energetic ions and reactive radicals interact over larger sheath distances (~ mm) with higher kinetic impact (10–100 eV). In contrast, AP surface discharge confines active metastable and ionic species to a thin active plasma layer (<0.1 mm) directly adjacent to the fibre surface at lower kinetic energies (1–3 eV), avoiding structural cell-wall degradation.

fabric which is later characterised. Using several DCSBD tiles, the method can be scaled up in width and process speed. [47].

2.4. Soxhlet extraction and characterisation

To quantify the surface wax content, a Soxhlet extraction (16 h washing in 150 ml hexane at 105 °C) was carried out on 5 g samples to remove the waxy substances from the raw FF fabric. The extracted material was analysed by chromatograph coupled with a mass spectrometer (GC–MS; Agilent 6890 series GC paired with an Agilent 5973 series mass selective detector). Chromatographic separation was achieved on a capillary column using helium as the carrier gas, and mass spectra were recorded under electron ionisation (EI) mode at 70 eV.

2.5. Contact angle measurement and surface analysis

Chemical surface composition was analysed by X-ray photoelectron spectroscopy (XPS, PHI 5600 LS; Mg K_α 1253.6 eV) at a take-off angle of 45°. Dynamic advancing contact angles were determined using a Krüss K100 tensiometer with a weight resolution of 1 μg. Three probe liquids, pure water, ethylene glycol, and diiodomethane (or 1-bromonaphthalene), were employed to evaluate the surface energy components of the fibres and coPOM films, following the Van Oss model as implemented by the method proposed by Della Volpe et al. [48] A detailed explanation of the procedure used to measure contact angles and calculate the surface energy components is provided in literature. [49,50].

2.6. Composite processing and sample preparation

FF thermoplastic composites were manufactured via film stacking using six pre-dried fabrics and seven pre-dried polymer films of a thickness of about 100 μm following the same compression moulding procedure reported in previous studies. [19,23]. The mould was placed in a 190 °C pre-heated press (Vogt P200T-2E, Germany) and a piston pressure was applied resulting in a cavity pressure of 1 MPa. After 10 min pressing at 190 °C, the mould was transferred to the cooling level of the press and pressure was re-applied and maintained during the cooling cycle. The number of films was selected to target a fibre volume fraction (FVF) of approximately 60%. The actual FVF was determined by quantitative image analysis of polished composite cross-sections, in which the fibre, matrix, and void phases were distinguished using ImageJ following the procedure reported previously, [19] yielding an FVF of around 61.2 ± 1.1%. Tension and compression test coupons were cut from the manufactured composites using a DIADISC 5200 (Mutronic Präzisionsgerätebau GmbH & Co. KG, Rieden, Germany) equipped with a diamond coated saw blade. Because of the complex geometry of the shear specimens and the importance to align the notches, the samples were cut using a Byjet 2 (Bystronic, Switzerland) water jet machine. To avoid delamination, the jetting point was set 10 mm outside of the specimen's desired contour. Polished composite cross-sections were imaged using an optical microscope (Keyence VR 5000). Representative images of untreated and AP plasma-treated composites were analysed in ImageJ using identical thresholding conditions to estimate the apparent area fraction of void/poorly impregnated regions.

2.7. Scanning electron microscopy

The morphology of the fibres was analyzed using scanning electron microscopy (SEM). Specimens were fixed on a holder with carbon tape and sputter coated to apply a 5 nm gold film with the high vacuum deposition system Leica EM ACE600. The coated specimens were then scanned using a TESCAN Vega 3 SEM.

2.8. Mechanical testing

The NF thermoplastic composites were tested on an universal material testing machine (Walter + Bai AG, Switzerland), equipped with a 100 kN capacity load cell. The untreated and AP-treated FF-reinforced composites were characterised for their tensile, compression and shear properties. Mechanical tests were carried out in accordance with ASTM D3039 for tensile, ASTM D3410 for compressive and ASTM D7078 for in plane shear. For the latter, unlike the also standardised Iosipescu test method (ASTM 5379), the V-notched rail shear test allows for a more effective load introduction due to the face loading and a larger zone of uniform shear stress between the notches. To determine the fibre and matrix dominated properties, tests were conducted for NF-composites with longitudinal (0°) and transverse (90°) fibre orientation. Specimens were clamped using a 6 bar pressure. To account for the clamping pressure, which is acting perpendicular to the loading direction, tension and compression specimens were supported by 2 mm thick glass fibre-reinforced end tabs, bonded to both ends of the samples.

To accurately measure the strain for the calculation of the moduli, a 50 mm clip-on extensometer was used for the tensile experiments. The compressive and shear specimens were equipped with strain gauges, type 1-LC11-3/120 and 1-XY4x-6/120 purchased at HBM^{TM} Switzerland. Strain gauges were bonded onto roughened and cleaned samples using a cyanoacrylate super glue, type Z70 (HBM^{TM} Switzerland). Statistical differences between the untreated and AP plasma-treated composites were evaluated separately for each mechanical property using one-way analysis of variance at a significance level of ($\alpha = 0.05$). Results are reported as the arithmetic mean ± one standard deviation based on three specimens per condition.

3. Results

3.1. *Effect of* treatments *on fibres*

3.1.1. *Plasma cleaning compared to boiling*

After the pre-boiling process (10 min acetone), Soxhlet extraction indicated that 0.15 wt% of waxes were left on the FF surfaces compared to an initial content of 0.42 wt%.. The LP plasma cleaning step (5 min CO_2/Ar plasma) performed with the raw FF fabrics resulted in 0.11 wt% and 0.12 wt% of residual wax for 700 W and 1000 W exposure, respectively. Likewise, XPS analysis on the raw, pre-boiled and fully boiled FF fabrics revealed an increasing O/C ratio by removal of carbon-rich waxy substances and exposure of the cellulosic materials (Table 1). Note that the full boiling process involves the removal of wax and pectin/lignin, which however does not add new functionalities at the fibre surface.

LP plasma cleaning of the FF fabrics (5 min CO_2/Ar plasma, 700 W) resulted in an O/C ratio of 0.39, which lies in between the O/C ratios measured for pre-boiled and boiled fabrics. The plasma cleaning with CO_2 is based on the formation of long-living atomic oxygen species in the gas phase, which is enhanced by energy transfer from excited Ar states. The interaction with (organic) hydrocarbons thus forms volatile CO, CO_2 and H_2O products responsible for the removal of the outermost wax layer. In addition, some oxygen is introduced in the modified surface forming hydroxyl/ether (C-OR), carbonyl (C=O) and carboxyl/ester (COOR) groups as identified by XPS analysis. Note that the open structure of the flax fabric favours penetration of the reactive plasma species at low pressure. [51] Together, the raw, pre-boiled, boiled, and LP-plasma-treated results provide a controlled reference for relating wax removal from plasma-induced surface functionalisation and for comparison with the AP plasma treatment results presented in Section 3.1.2.

Plasma functionalisation is known to undergo aging effects involving the decay of short-lived species (e.g. free radicals), re-orientation of polar groups, and migration of low molecular weight species. [52] This effect can be reduced via the removal of wax layers. Residual wax, however, might still migrate and functional groups induced at the surface might re-orient leading to a reduction in surface functionality. Such effects equilibrate, i.e. the surface gets stabilised over time, typically within days. [53] Interestingly, storage for three months at ambient conditions (23 °C, 65% RH) only showed minor aging effects, maintaining the observed O/C ratio. The applied plasma cleaning thus appears to be a promising treatment for the functionalisation of FF. Extended plasma exposure time (10 min) or enhanced power (1000 W), however, neither increase the measured O/C ratio further (maintained around 0.4), nor removed more waxy substances, as seen by Soxhlet extraction. The surface of the FF still appeared smooth after the CO_2 plasma etching (Fig. 2), avoiding damaging of the fibre as observed for low-pressure O_2 plasma etching. [32] Despite the images showing only one side of the fibre, significant changes of the surface morphology were not found when comparing all sides.

Table 1
Composition and C1s detail spectrum of ampliTex UD (ampUD) FF in raw condition, pre-boiled before fibre spinning and boiled a second time after fibre spinning.

Sample	Composition (at%)			C1s detail spectrum (at%)			
	C	O	O/C	C–C	C–O	C=O	COOR
ampUD (raw)	83.3 ± 1.4	16.7 ± 1.4	0.21	81	13	6	~0
ampUD (pre-boiled)	78.7 ± 1.3	21.3 ± 1.3	0.27	71	20	8	~1
ampUD (boiled)	67.6 ± 1.8	32.4 ± 1.8	0.48	54	32	13	~1

3.1.2. *Plasma cleaning with FF fabrics*

As the cleaning effect of the plasma on the surface of the raw FF was found to be limited, i.e. leaving around 0.1 wt% of waxy substances, FF fabrics were used in the following to investigate the potential for further removal of wax layers by LP and AP plasmas. This approach would still strongly reduce time, energy, and chemicals by replacing the alkali boiling with a dry plasma treatment. Indeed, the LP CO_2 plasma cleaning (5 min, 700 W) performed after pre-boiling noticeably enhanced the removal of residual waxes as seen by the high O/C ratio (Table 2), which corresponds to cellulosic materials. Using two layers of FF fabrics and measuring the elemental composition on the lower, covered FF placed at the drum resulted in a small reduction in O/C ratio. The plasma cleaning effect was thus confirmed to show a good penetration and introduction of functional groups into the textile structure. Therefore, the applied plasma treatment from only one side can be considered as sufficient. Likewise, the reduction of plasma exposure time to 1 min still allowed a high O/C ratio and high functional group density when using pre-boiled FF fabrics.

Since the production of composites requires elevated temperatures, the plasma-cleaned fabric was exposed to 170 °C in a standard hot-air oven for one hour to investigate the effect of thermal exposure on migration and re-orientation processes. It was found that the heating procedure reduced the O/C ratio, probably due to surface migration of residual waxes, and induced a drop in the functional group density at the surface. The observed values by XPS (O/C ≈ 0.50, [COOR] ≈ 3 at%), however, were still higher compared to the full boiling procedure (O/C ≈ 0.48, [COOR] ≈ 1 at%). Furthermore, it can be expected that the functional groups become stabilised once reacted, e.g., with the matrix of the composite material.[54] Plasma cleaning using pre-boiled FF fabric thus seems to be well suited for composite materials.

AP plasma cleaning in air was applied to obtain a comparison with the LP plasma results, and to demonstrate ways to facilitate industrial implementation based on a continuous R2R process at ambient conditions. At first, a 5 min treatment was carried out with the pre-boiled FF fabric moving slowly over the area of the Diffuse Coplanar Surface Barrier Discharge (DCSBD) device. Due to the plasma volume extending about 0.3 mm above the electrode, some penetration of reactive species into the fabric structure can be expected. Indeed, this treatment gave the highest O/C ratio of 0.74 and also the highest functional group density. Therefore, the plasma exposure time can be shortened to enable a faster process. A 30 s treatment time still allowed an appropriate functionalisation of the FF fabric. Hence, the exposure time was finally reduced to 10 s for treating several meters of FF fabric of 400 mm width in a roll-to-roll process. Using just two DCSBD devices next to each other to cover a width of 400 mm with a length of 80 mm, a process velocity of 0.5 m/min was thus reached. Addition of such plasma devices in one line has the potential to further increase the process velocity. [47] Most of all, a still high O/C ratio was observed indicative for improved removal of waxes accompanied by the introduction of functional groups.

3.2. *Surface energy analysis of FF*

The measured advancing contact angles of different probe liquids for the untreated, LP and AP plasma-treated FF, as well as the coPOM polymer, are presented in Table 3. The reduced contact angles with water observed for both plasma-treated fibres indicate enhanced

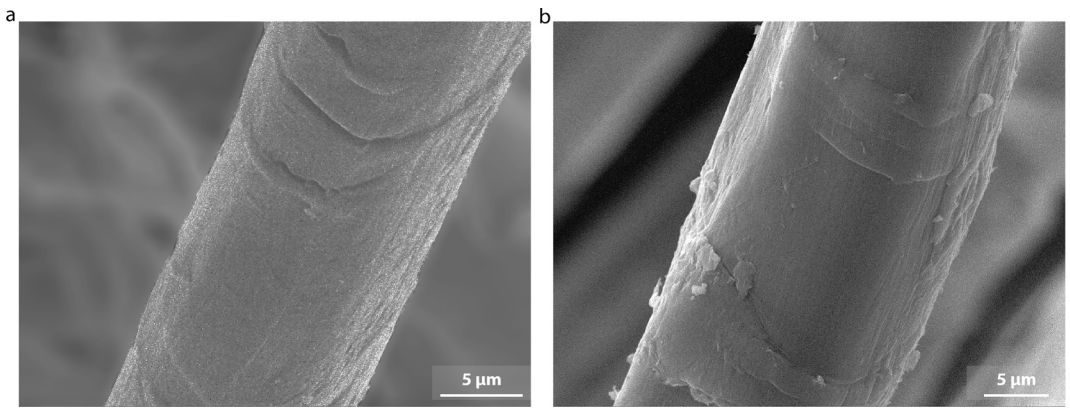


Fig. 2. Scanning electron microscopy images of (a) untreated and (b) CO_2/Ar LP plasma, 1000 W treated ampliTex® UD FF.

Table 2
Composition and C1s detail spectrum of pre-boiled ampliTex UD (ampUD) FF fabrics with plasma treatments.

Sample	Composition (at%)			C1s detail spectrum (at%)			
	C	O	O/C	C–C	C–O	C=O	COOR
LP plasma (CO_2, 700 W, 5 min)	58.9 ± 1.2	41.1 ± 1.2	0.69	40	36	17	7*
LP plasma (CO_2, 700 W, 5 min) covered FF fabric	60.5 ± 1.6	39.5 ± 1.6	0.65	45	30	19	6*
LP plasma (CO_2, 700 W, 1 min)	62.2 ± 1.0	37.8 ± 1.0	0.61	41	35	17	7*
LP plasma (CO_2, 700 W, 1 min) 170 °C heat treated	66.6 ± 1.4	33.4 ± 1.4	0.50	51	31	15	~3
AP plasma (air, 350 W, 5 min)	57.5 ± 1.2	42.5 ± 1.2	0.74	30	37	24	9*
AP plasma (air, 350 W, 30 s)	61.4 ± 1.2	38.6 ± 1.2	0.63	40	36	19	5*
AP plasma (air, 370 W, 10 s – continuous 0.5 m min^{-1})	62.9 ± 1.5	37.1 ± 1.5	0.59	43	38	16	3*

* High COOR value suggests the addition of functional groups on the surface.

hydrophilicity, likely resulting from the removal of surface waxes. This finding is consistent with the increased O/C ratio and higher concentrations of oxygen-containing functional groups shown in Table 2. Compared with the CO_2-based LP plasma treatment, the O_2-based AP plasma treatment leads to a more pronounced increase in the total surface energy γ_{tot}. This is because both dispersive component γ_{LW} and polar component γ_{ab} of the AP plasma-treated fibres were increased, whereas the LP plasma treatment only increased γ_{LW}. For the LP CO_2/Ar treatment, the increase in γ_{LW} can be attributed to the removal of non-polar waxy surface layer and exposure of the underlying cellulosic surface, which alters the dispersive interactions. The low γ^+ values indicate weak electron-acceptor (Lewis-acid) character, with associated small absolute error reflecting reproducibility of such low γ^+ values. The higher γ_{ab} observed for the AP plasma-treated fibres is probably due to the presence of a high concentration of O_2 in the reactor chamber as well as a contribution of moisture at ambient conditions. Electron-impact dissociation of O_2 may produce reactive atomic oxygen, while ambient water vapour may contribute to the formation of OH radicals. [55,56] Atomic oxygen can subsequently react with O_2 to form O_3.[55–57] These reactive oxygen species can oxidize the outer fibre surface and increase the abundance of oxygen-containing functionalities such as C–O, C=O and O–C=O groups, thereby increasing the polar interactions contributing to γ_{ab}.

The theoretical work of adhesion and the spreading coefficient, calculated based on the surface energy components, are critical parameters for evaluating the potential physical interactions between the fibres and the matrix. The former is used to assess the adhesive strength between the fibre and matrix, while the latter serves as an indicator of wetting behaviour. The increased work of adhesion observed for both plasma treatments suggests enhanced interfacial bonding, which is particularly prominent for the fibres treated by AP plasma, as presented in Fig. 3. The trend in the spreading coefficients aligns well with that of the work of adhesion. The negative spreading coefficient (−3.9 mJ/m^2) of untreated fibres demonstrates imperfect wetting by the polymer matrix. In contrast, the LP and AP plasma-treated fibres show positive spreading coefficients, suggesting the possibility of complete and spontaneous wetting by the liquid polymer. The improved wetting was also reflected in the representative composite cross-section images shown in Fig. 3 (b-c). The untreated composite exhibited more pronounced void/poorly impregnated regions between the fibre bundles, whereas the AP plasma-treated composite showed a more uniform matrix distribution. Image analysis of the cross-sections yielded apparent

Table 3
Contact angles and surface energy components of different types of fibres and coPOM.

Materials	Contact angles (°)				Surface energy components* (mJ/m^2)				
	W*	EG*	DIM*	BRN*	γ^{tot}	γ^{LW}	γ^{ab}	γ^+	γ^-
Untreated	75.6 ± 5.4	58.4 ± 3.0	63.6 ± 5.2	–-	29.4 ± 3.6	26.5 ± 0.5	2.9 ± 1.5	0.3 ± 0.5	6.1 ± 0.7
LP plasma	55.2 ± 5.6	55.6 ± 4.2	52.1 ± 6.2	–-	33.3 ± 2.5	33.1 ± 1.6	0.2 ± 2.6	0.001 ± 0.01	15.7 ± 1.4
AP plasma	56.4 ± 7.7	36.1 ± 7.1	–-	32.3 ± 8.8	41.8 ± 4.2	37.8 ± 3.4	4.0 ± 2.4	0.4 ± 0.4	10.9 ± 4.3
coPOM	86.1 ± 0.8	65.2 ± 0.8	54.3 ± 1.4	–-	31.9 ± 0.8	31.8 ± 0.8	0.09 ± 0.2	0.001 ± 0.00	2.1 ± 0.2

* W- water, EG – ethylene glycol, DIM – diiodomethane, BRN – 1-bromonaphtalene; γ^{tot} – total surface energy, γ^{LW} – Lifshitz-van der Waals (dispersive) component, γ^{ab} – acid-base (polar) component, γ^+ – acid component, γ^- – base component. For AP plasma-treated fibres, 1-bromonaphthalene was used as the non-polar probe instead of diiodomethane. In the Della Volpe–Siboni parametrisation both liquids are purely dispersive and therefore interchangeable as apolar probes; this substitution does not alter the conditioning (coordination number) of the liquid triplet, which remains a well-posed set for the determination of the surface energy components, so the results are directly comparable at the level of trends while only minor shifts in absolute values may occur due to the different liquid surface tensions. [58].

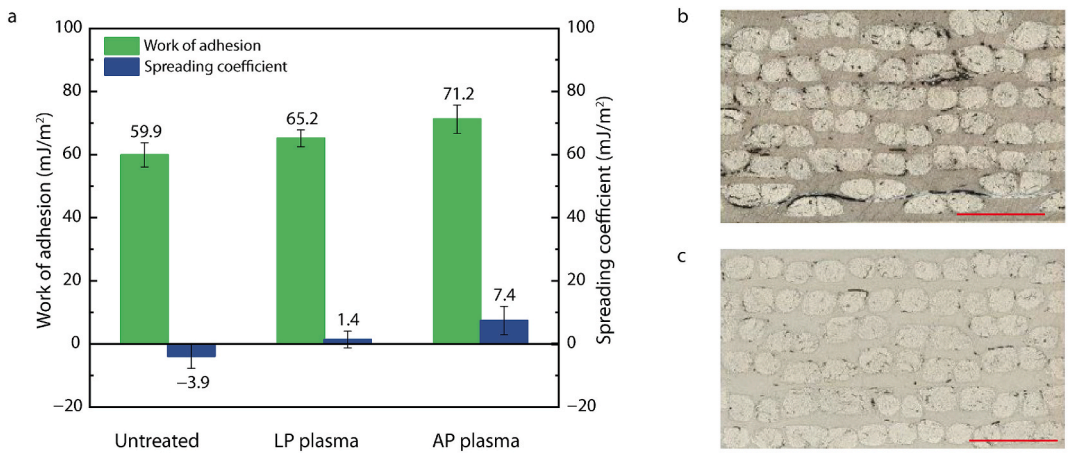


Fig. 3. (a) The work of adhesion and spreading coefficient of untreated and plasma-treated fibres with coPOM polymer. (b-c) Representative polished cross-sectional micrographs of (b) untreated and (c) AP plasma-treated FF-coPOM composites. The scalebars indicate 1 mm.

void/poorly impregnated area fractions of approximately 3.1% and 0.4% for the untreated and AP plasma-treated composites, respectively, supporting improved impregnation following AP plasma treatment.

Based on the surface analyses presented in Sections 3.1 and 3.2, the continuous AP treatment at 0.5 m/min (10 s exposure, O/C ≈ 0.59) was selected for the composite laminate fabrication. Although longer treatments produced higher O/C ratios (0.63 at 30 s and 0.74 at 5 min), the 10 s treatment retained substantial surface functionalisation and resulted in a positive spreading coefficient, while enabling a considerably higher continuous processing speed. The present study therefore evaluates the composite performance only for this selected processing condition. A comparative optimisation of composite properties across different AP exposure times was not performed. Consequently, only AP plasma-treated fibres were employed in the fabrication of composites

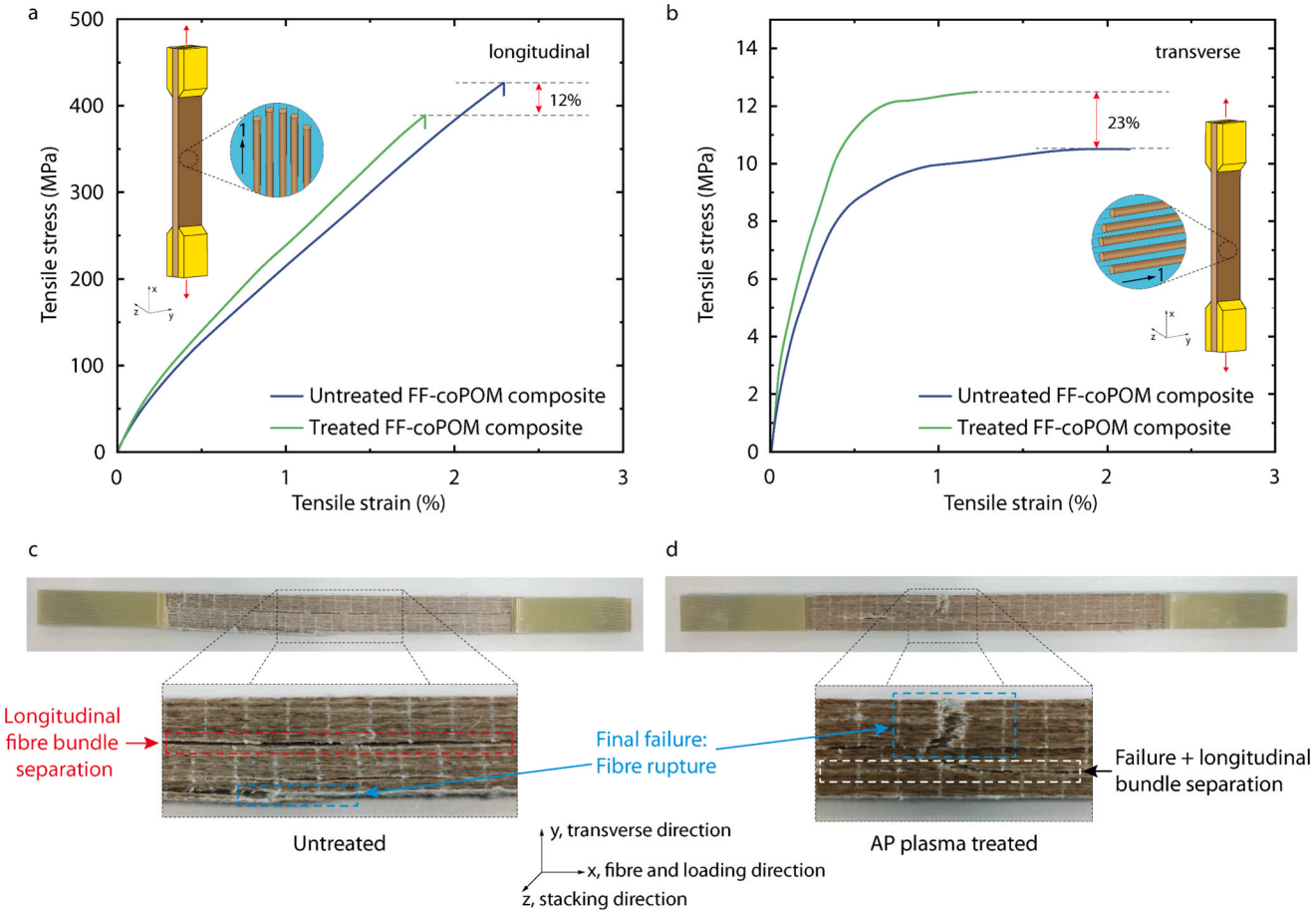


Fig. 4. Tensile test of the untreated and treated FF-coPOM composites. (a-b) Stress–strain diagram of the specimens tested in longitudinal and transverse directions, respectively. Shown are representative curves from the sample of eight tensile specimens for each configuration. (c-d) Failure behaviour of (c) untreated and (d) AP plasma treated FF-coPOM composites, tested in longitudinal direction. The dashed boxes show longitudinal fibre separation (red), fibre rupture (blue), and rupture + bundle separation (white) observed in the specimens.

and in the mechanical tests discussed in Section 3.3.

3.3. Mechanical properties

To gauge understanding of the effect of atmospheric plasma treatment on the mechanical behaviour, a comprehensive mechanical characterisation of the composite specimens were performed.

3.3.1. Tension

The tensile properties are key for the design of structural materials. The reported values illustrate the load carrying ability of NFs embedded in polymeric matrices and may allow the assessment of the stress transfer to adjacent fibres in case of premature fibre damage. [59,60] In the event of localised fibre failure, stresses are redistributed via shear deformation of the matrix maintaining the load carrying ability of the composite. This shows that the fibre/matrix interface, enhanced by the plasma treatment, is strong enough to withstand those stresses. Fig. 4 (a) shows representative stress–strain curves for tensile FF-coPOM matrix composites tested in the longitudinal direction. The longitudinal tensile elastic moduli, E_{t1}, of the untreated and AP plasma treated composites were measured to 28 GPa and 31 GPa, respectively. The tensile strengths were measured to be 433 MPa for the untreated and 382 MPa for the AP plasma treated coPOM matrix composites. The modulus could be enhanced by ~ 12%, whereas the strength was found to be adversely affected by the treatment – a strength reduction of 12% was recorded. This can be explained by the improved wetting leading to better impregnation, at the sacrifice of some fibre damage occurring during the treatment when applying an air AP plasma. Independent of the fibre preparation, the specimens tested in the longitudinal direction failed in a brittle manner by either fibre failure or longitudinal fibre separation. Although longitudinal splitting was observed in some specimens, it did not result in a distinct premature load drop before the maximum load. The reported longitudinal tensile strength therefore represents the maximum axial stress sustained by the coupon and should be interpreted as a coupon-level axial load capacity rather than a pure fibre-rupture tensile strength.

Fig. 4 (b) shows representative stress–strain curves for tensile FF-coPOM matrix composites tested in the transverse direction. The transverse tensile elastic moduli, E_{t2}, were measured to 1.5 GPa and 2.5 GPa for the untreated and treated specimens, respectively. The transverse strengths were measured to 10.6 MPa for the untreated and 12.7 MPa for the treated composite specimens. These values represent an increase of about 67% and 23% in modulus and in strength, respectively. Unlike the longitudinal failure behaviour, the transverse failure mode is strongly affected by the nature of the matrix material and the fibre–matrix adhesion. The curves in Fig. 4 (b) illustrate a very ductile material behaviour indicated by the plateau at maximum stress over a range of at least 1% tensile strain which is consistent with work reported previously. [19].

Interestingly, the untreated samples showed a different failure mode compared to the samples with the AP plasma treatment. As depicted in Fig. 4 (c), longitudinal fibre bundle debonding occurred prior to fibre failure in the untreated specimens. Although not accompanied by a sudden load drop, this failure sequence was distinctive for the composites without the fibre surface treatment. Conversely, the final failure of the AP plasma treated samples is characterised by large zones of ruptured fibres (Fig. 4 (d)). In contrast to the fibre-dominated longitudinal properties, the transverse composite performance can provide a much better insight into the adhesion between the fibres and the matrix, and what effect the AP plasma treatment has on the interface properties.

3.3.2. Compression

Fig. 5 (a) shows representative compressive stress–strain curves for FF-coPOM matrix composites tested in the longitudinal direction. The longitudinal compressive moduli, E_{c1}, for the untreated and AP plasma treated coPOM matrix composites are not reported because the strain-gauge response was inconsistent during the initial loading region, preventing a reliable determination of the initial elastic slope. The longitudinal compressive strengths, $\sigma_{c1_{max}}$, were measured to 120 and 129 MPa for the untreated and treated coPOM matrix composites, respectively. The average compressive strength was increased by 8%.

Fig. 5 (b) shows representative compressive stress–strain curves for FF-coPOM matrix composites tested in transverse direction. The transverse compressive moduli, E_{c2}, were measured to 1.2 and 1.75 GPa for untreated and AP plasma treated composites. Although the absolute difference is ultimately small, the increase in modulus due to the AP plasma treatment was found to be 46%. A similarly high increase of 43% was measured for the ultimate compressive strengths. The average strengths were determined to be 50 and 71 MPa for the untreated and treated coPOM matrix composites, which indicates a positive effect of the AP plasma process on the interface formation. The improvement in compressive properties after AP plasma treatment can be attributed to enhanced fibre–matrix adhesion. Better interfacial bonding may help support the fibres during longitudinal compression and reduce premature fibre–matrix separation, while in transverse compression it can improve load transfer across the fibre–matrix interface.

3.3.3. Shear

Fig. 5 (c) shows representative shear stress–strain curves for FF-coPOM matrix composites tested in the longitudinal direction. The in-plane shear moduli, G_{12}, of untreated and AP plasma treated composites were measured to 4.3 and 4.9 GPa, respectively, which represents an increase of 15%. The longitudinal shear strengths, $\tau_{12_{max}}$, were found to be 27 and 33 MPa for the untreated and treated composites, respectively. The strength enhancement due to the fibre treatment was calculated to 23 %.

Fig. 5 (d) shows representative shear stress–strain curves for FF-coPOM matrix composites tested in the transverse direction. The transverse in-plane shear moduli, G_{21}, of untreated and AP plasma treated composites were measured to 3 and 3.9 GPa, respectively. This illustrates an enhancement of 31%. The transverse shear strength, $\tau_{21_{max}}$, was measured to be 18 and 22 MPa, respectively, which represents an increase of 19%.

As can be seen from the stress–strain curves in Fig. 5 (c) and (d), the response of the untreated and treated samples to the applied force is very similar. The difference lies in the stress magnitude where a deviation from a linear-elastic material behaviour occurs. This deviation relates in this case to the measured strength and is 23% and 19% higher for the AP plasma treated composites in longitudinal and transverse direction, respectively.

The AP plasma treated samples with the fibre orientation in the transverse direction (green curve in Fig. 5 (d)) failed in a very special manner, i.e. buckling of the surface layer. The out-of-plane failure caused the surface bonded strain gauge to peel off. Hence, the maximum strain range could not be reached. Therefore, the ultimate shear stress has been extracted from the stress-displacement data recorded by the machine's load cell and the cross-head movement.

3.3.4. Summary

As illustrated in the engineering constants summarised in Table 4, one can clearly identify the positive effect of the AP plasma treatment on mechanical properties of the coPOM matrix composites. The transverse properties, particularly the tensile, compressive and shear moduli benefit significantly from the treatment. Improvements of up to 67 % were measured.

The increases in the in-plane moduli can be visualised in form of property polar diagrams Fig. 6 (a) and (b) show the elastic and shear modulus, respectively, as a function of the fibre angle. One can note that the green envelopes, which represent the property area for the coPOM matrix composites with the AP plasma fibre treatment, are bigger, which results in a larger design space for stiffness driven designs.

Failure criteria can be used to describe the failure behaviour of UD-

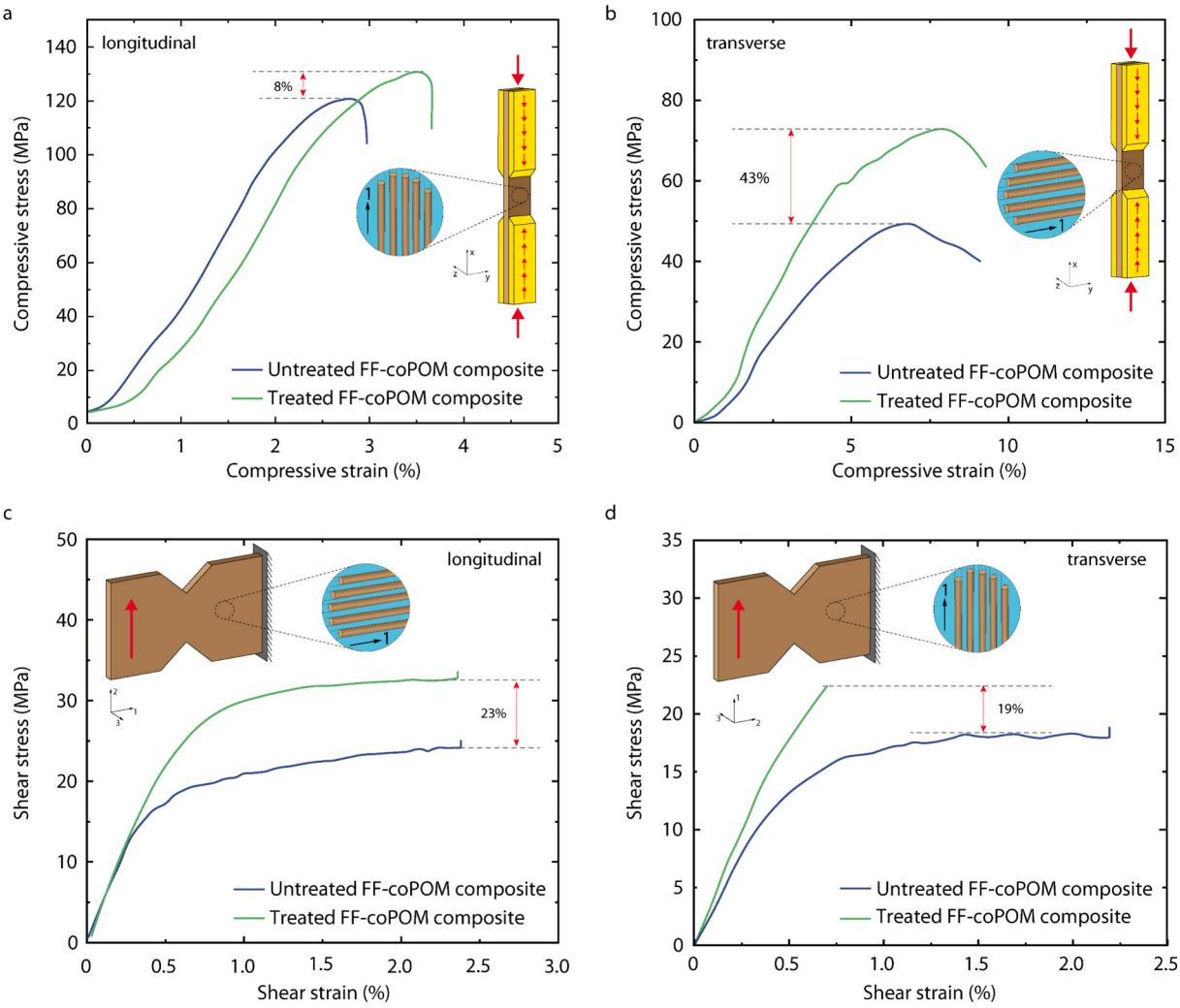


Fig. 5. Compression and shear stress–strain diagrams of the untreated and atmospheric-pressure (AP) plasma treated coPOM matrix composites. (a-b) In compression with (a) longitudinal and (b) transverse fibre orientation. The offset of 0.5% strain in (a) was added to distinguish the two curves. (c-d) In shear with (c) longitudinal and (d) transverse fibre orientation. (Shown are representative curves from the set of eight tensile specimens for each configuration).

Table 4
Mechanical properties of FF-reinforced coPOM matrix composites (FVF 61.2 vol%). Comparison of composite properties without and with atmospheric pressure plasma treated fabrics prior to processing. The values represent mean ± one standard deviation for $n = 3$ specimens per condition. Differences between the untreated and the AP plasma-treated composites were evaluated separately for each mechanical property using one-way analysis of variance (ANOVA) at $\alpha = 0.05$; '*ns*' indicates $p \geq 0.05$.

Materials		FF-reinforced coPOM	AP plasma treated FF-reinforced coPOM	Enhancements in average properties	Statistical significance (ANOVA p value)
Tension					
Longitudinal	E_1(GPa)	28.2 ± 0.7	31.5 ± 0.9	12%	0.007
	σ_{1max}(MPa)	433 ± 8.4	382 ± 10.8	− 12%	0.003
Transverse	E_2(GPa)	1.5 ± 0.2	2.5 ± 0.2	67%	0.004
	σ_{2max}(MPa)	10.35 ± 0.6	12.7 ± 0.4	23%	0.005
Compression					
Longitudinal	σ_{c1max}(MPa)	119.6 ± 2.2	129.3 ± 1.4	8%	0.003
Transverse	E_{c2}(GPa)	1.2 ± 0.1	1.75 ± 0.4	46%	0.082, *ns*
	σ_{c2max}(MPa)	49.7 ± 4.6	70.9 ± 3.0	43%	0.003
Shear					
Longitudinal	G_{12}(GPa)	4.26 ± 0.2	4.93 ± 0.1	15%	0.007
	τ_{12max}(MPa)	26.5 ± 1.3	32.7 ± 2.8	23%	0.025
Transverse	G_{21}(GPa)	3.0 ± 0.1	3.92 ± 0.1	31%	< 0.001
	τ_{21max}(MPa)	18.11 ± 0.9	21.6 ± 1.4	19%	0.022

reinforced composites. With the application of such criteria, it is possible to construct failure envelopes in the stress space that can define the combinations of stresses leading to failure. Fig. 6 (c) shows a 3D representation of the failure envelope determined using Puck's failure criterion under in-plane stress-state (σ_1, σ_2, τ_{12}). [61,62] Using this criterion, one can distinguish between fibre and inter-fibre failure. The

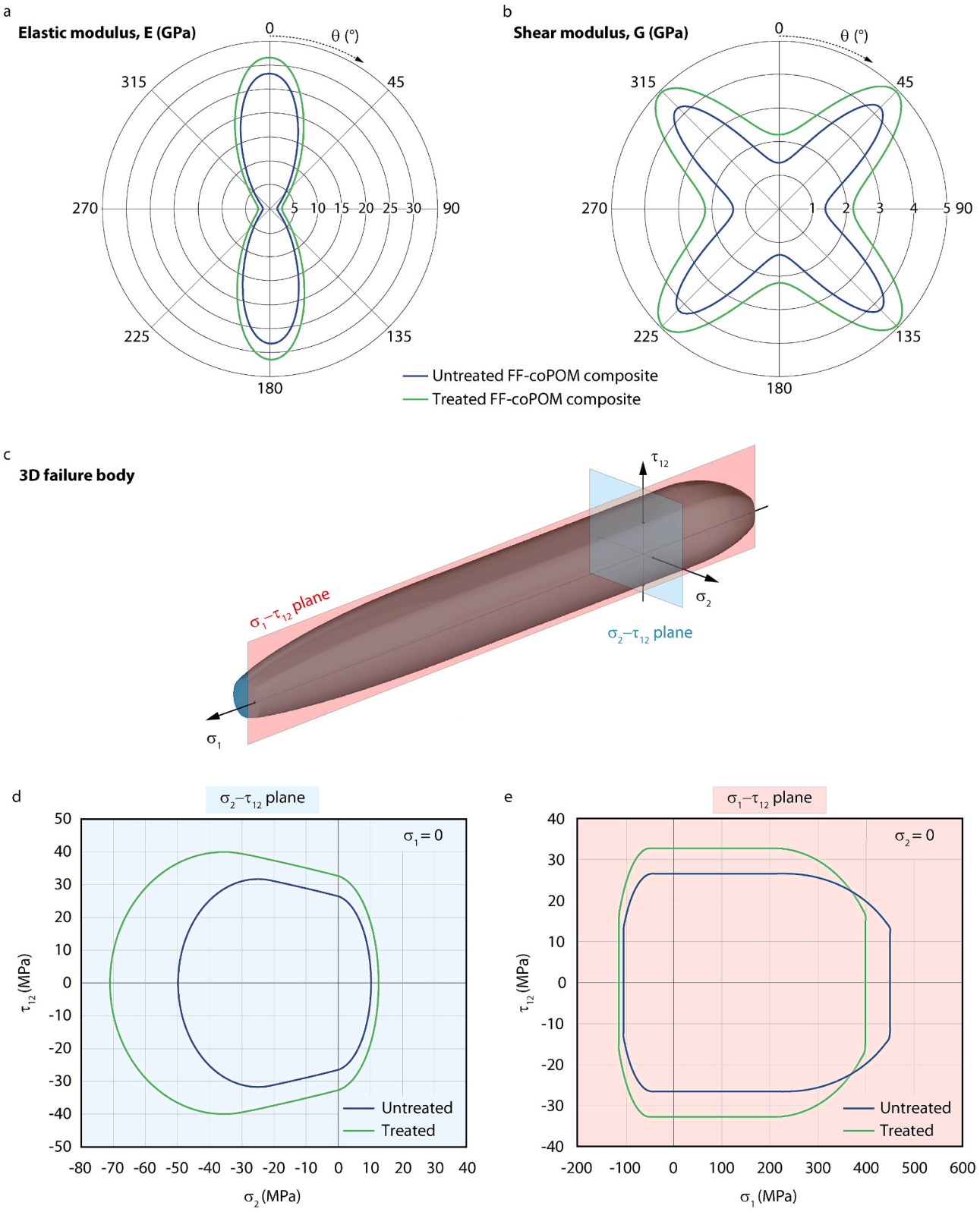


Fig. 6. Summary of the results. (a-b) Polar diagram of in-plane engineering elastic constants: (a) Elastic modulus, *E* and (b) Shear modulus, *G*. (c-d) Failure envelopes of untreated and AP plasma treated coPOM matrix composites. (c) 3D failure body determined using Puck's inter-fibre failure criterion [61] (generated with eLamX 2.5), (d) failure envelope in the $\sigma_1 - \tau_{12}$ plane, and (e) failure envelope in the $\sigma_2 - \tau_{12}$ plane (generated with ESAComp 4.7).

experimentally measured strength values reported in Table 4 were used as the material strength inputs for the Puck analysis. The calculations considered the in-plane stress state ($\sigma_1, \sigma_2, \tau_{12}$) of the UD composite, and no additional interaction parameters were fitted to the present experimental data. the Puck implementations available in eLamX 2.5 and ESAComp 4.7 were used to construct the envelopes. Fig. 6 (d) shows the areas for inter-fibre failure ($\sigma_1 = 0$) for the untreated (blue) and AP plasma treated (green) coPOM matrix composites. This figure depicts that in the AP plasma treated composites, higher stresses can be sustained in both transverse tension and compression, but more prominently in transverse compression. For the case of $\sigma_1 \neq 0$, i.e. the composite under longitudinal tension or compression, slices parallel to the $\sigma_2 - \tau_{12}$ plane describe the areas for inter-fibre failure. In addition to the inter-fibre case, the fibre failure criteria for tension and compression were added (Fig. 6 (e)). The longitudinal tensile input corresponds to the maximum coupon stress reported in Section 3.3.1 and therefore represents a coupon-level axial failure limit rather than an intrinsic fibre-rupture strength. Accordingly, the calculated failure envelopes are used primarily as a comparative representation of the untreated and plasma-treated composites rather than as independently validated multiaxial failure predictions.

4. Discussion

4.1. Plasma-induced surface modification and implications for wetting/adhesion

The surface analysis demonstrates that both low-pressure (LP) CO_2/Ar and atmospheric-pressure (AP) air plasmas modify the outermost FF surface by (i) removing carbon-rich waxy species and (ii) increasing the concentration of oxygen-containing functional groups. This is evidenced by the rise in O/C ratio and the redistribution of the C1s components toward C-O, C=O and COOR contributions after plasma exposure (Table 2). The removal of waxes is particularly relevant for FF, where a thin (nm-scale) hydrophobic layer can dominate wetting and interfacial behaviour despite its small mass fraction.

These chemical modifications translate into improved fibre-coPOM wetting potential. The AP plasma treatment produces the largest increase in total surface energy (γ^{tot}) and, more importantly, increases both dispersive (γ^{LW}) and polar (γ^{ab}) components (Table 3). In contrast, the LP plasma treatment predominantly increases the dispersive contribution. The thermodynamic indicators derived from these surface-energy components further support the improvements in wetting/adhesion: the work of adhesion increases for both the plasma treatments, and the spreading coefficient changes from negative for untreated FF (imperfect wetting) to positive (spontaneous wetting) for the plasma treated fibres (Fig. 3). This suggests the possibility of complete wetting by molten coPOM during consolidation. Taken together, the XPS and surface-energy analysis provide a consistent mechanistic basis for expecting stronger interfacial interactions and a more efficient stress transfer in the plasma-treated composites.

An important consideration for thermoplastic processing is surface stability at elevated temperatures. The reduction in O/C ratio after heating the plasma-cleaned FF at 170 °C indicates partial surface restructuring, involving the reorientation of polar moieties and/or migration of the residual low molecular weight species away from the outer surface. [53,63] Nevertheless, the surface remains more oxygen-rich than the boiled FF, indicating that the plasma treated state is not fully erased by thermal exposure and can still contribute to interfacial development during the melt impregnation. This is consistent with the substantial changes observed in the mechanical properties after AP treatment.

4.2. Coupon-scale mechanical responses

The mechanical characterisation results shows that the AP plasma treatment improves the composite response most strongly in loading modes governed by the matrix and the fibre/matrix interface. Pronounced increases are measured in transverse tension ($E_2 \sim 67\%$, $\sigma_{2max} \sim 23\%$), transverse compression ($E_{c2} \sim 46\%$, $\sigma_{c2max} \sim 43\%$), and in-plane shear in both the transverse and longitudinal directions ($G_{12} \sim 15\%$, $\tau_{12max} \sim 23\%$; $G_{21} \sim 31\%$, $\tau_{21max} \sim 19\%$) (Table 4). The enlargement of the inter-fibre failure domain under transverse and shear loading (Fig. 6 c-e) is consistent with the higher work of adhesion and positive spreading coefficients derived in Section 3.2, which indicate thermodynamically more favourable wetting and interfacial bonding. Further, the polar diagrams (Fig. 6 a-b) illustrate an extended design space of the modulus for the treated composites, which is particularly relevant for structural design where off-axis stiffness and shear properties often limit the performance more compared to the modulus along the fibre direction.

The failure-envelope analysis provides additional support to this interpretation. The treated composite exhibits a larger inter-fibre failure domain predicted by Puck's failure criterion, especially, under transverse compression and in the combined transverse/shear states (Fig. 6 c-e). Since transverse compression and shear are highly sensitive to interfacial integrity, the observed envelope expansion is consistent with enhanced resistance to interfacial damage initiation and propagation.

4.3. Trade-off in longitudinal tensile strength and change in failure sequence

In contrast to the improvements in transverse and shear behaviour, the AP plasma-treated composite showed a reduction in longitudinal tensile strength ($\sigma_{1max} \sim$ -12%), despite a moderate increase in the longitudinal modulus ($E_1 \sim +12\%$) (Table 4). This divergence between stiffness and strength is not unexpected in UD composites with high FVF. E_1 is primarily governed by the fibre stiffness and load sharing, whereas σ_{1max} is strongly influenced by the variability in fibre strength, its distribution, defects, and the nature of the evolution of damage before final failure. [59,64] Again, improved adhesion can alter the micro-scale failure sequence in a way that reduces the apparent macroscopic tensile strength. The untreated composites exhibit longitudinal fibre-bundle debonding prior to the final failure (Fig. 4 c). It may act as a progressive damage mechanism that redistributes the load and delays the catastrophic rupture. [65–67] After AP treatment, fracture surfaces show larger zones of ruptured fibres (Fig. 4 d), which is consistent with the suppression of early interfacial sliding/debonding. In such a scenario, the composite may transition from a more gradual damage evolution to a more unstable, fibre-rupture dominated final failure, particularly once a critical cluster of fibres fail. This interpretation aligns with the observation that AP treatment improves the off-axis properties (where debonding is detrimental) while potentially reducing damage tolerance under fibre-direction tension, where limited interfacial slip can sometimes delay the catastrophic failure. We conjecture that fibre damage induced by the plasma treatment may also contribute to the observed strength reduction. Previous studies on plasma-treated flax fibres have reported slight reductions in fibre tensile strength after plasma exposure, particularly under oxygen-containing plasma conditions. [27,65,68] Oxygen-rich AP plasmas can modify the fibre surface through oxidation and etching, which under sufficiently aggressive treatment conditions may introduce surface defects and weaken the fibres.

4.4. Implications for processing and optimisation

From the application perspective, an important outcome is that AP plasma treatment leads to measurable improvements in the coupon-level mechanical property values for a NF thermoplastic composite system. More importantly, the developed route is compatible with roll-to-roll processing. The results also highlight that the optimal interface is application dependent: maximizing the interfacial strength improves the transverse tensile, compressive, and shear performance. However, it

may not maximize the fibre-direction tensile strength if fibre weakening or a reduction in progressive damage tolerance occurs. Consequently, optimisation of the AP plasma parameters (power density, exposure time, gas composition, stand-off distance, and thermal management) should aim to preserve fibre tensile integrity while retaining sufficient activation to improve the wetting and inter-fibre failure resistance. Establishing this optimised window might be the key towards translating plasma-enabled interfacial engineering into robust structural performance.

5. Conclusions

Atmospheric pressure plasma treatment effectively modifies the flax yarn surface by removing waxy species and increasing oxygen-containing functionalities, leading to improved wetting and enhanced flax fibre yarn-coPOM interfacial interactions. These surface modifications translate into significant improvements in the coupon-level mechanical properties in both matrix-dominated and interface-dominated loading modes. It includes improvements in the transverse tension and compression, as well as the in-plane shear properties, and is reflected by an expansion of the inter-fibre failure domain. In contrast, a reduction in the longitudinal tensile strength is observed despite an increase in the longitudinal modulus, indicating a trade-off between the enhanced interfacial load transfer and the reduced ability to accommodate damage progressively under fibre-direction loading. Considering structural loading scenarios, the benefit of improved compression performance and interfacial properties will likely outweigh the minor reduction of tensile properties. Overall, the results demonstrate that atmospheric-pressure plasma treatment provides a roll-to-roll-compatible route to expand the off-axis mechanical performance of flax fibre-thermoplastic coPOM composites, while highlighting the need for accurate optimisation of the plasma parameters to balance interfacial enhancement and composite tensile integrity.

CRediT authorship contribution statement

W. Woigk: Writing – review & editing, Writing – original draft, Investigation, Formal analysis, Conceptualization. **S. Patranabish:** Writing – review & editing, Writing – original draft, Investigation, Formal analysis. **J. Hao:** Writing – review & editing, Investigation, Formal analysis. **J. Rion:** Writing – review & editing, Funding acquisition, Conceptualization. **A.W. van Vuure:** Writing – review & editing, Funding acquisition, Conceptualization. **C. Dransfeld:** Writing – review & editing, Funding acquisition, Conceptualization. **D. Hegemann:** Writing – review & editing, Writing – original draft, Funding acquisition, Formal analysis, Conceptualization. **C.A. Fuentes:** Writing – review & editing, Writing – original draft, Formal analysis, Conceptualization. **K. Masania:** Writing – review & editing, Writing – original draft, Funding acquisition, Formal analysis, Conceptualization.

Declaration of competing interest

The authors declare that they have no known competing financial interests or personal relationships that could have appeared to influence the work reported in this paper.

Acknowledgements

This research project was financially supported by the Innosuisse Swiss Innovation Agency through project 15091.1 PFIW-IW HIPET-CONF. Further we would like to thank B. Frisch and C. Fab for the fruitful discussions. M. Černák, Masaryk University, Brno, Czech Republic is acknowledged for providing DCSBD devices.

Data availability

Data will be made available on request.

References

[1] P. K. Mallick, *Fiber-reinforced composites: materials, manufacturing, and design*, CRC press, 2007.
[2] D. B. Miracle, S. L. Donaldson, S. D. Henry, C. Moosbrugger, G. J. Anton, B. R. Sanders, N. Hrivnak, C. Terman, J. Kinson and K. Muldoon, *ASM handbook*, ASM international Materials Park, OH, 2001.
[3] Luo T, Hu Y, Zhang M, Jia P, Zhou Y. Resour Chem Mater 2024:100085.
[4] Dallaev R, Papež N, Allaham MM, Holcman V. Polymers 1981;2025:17.
[5] Prasad V, Alliyankal Vijayakumar A, Jose T, George SC. Sustainability 2024;16:1223.
[6] Capretti M, Del Bianco G, Giammaria V, Boria S. Materials 2024;17:2246.
[7] Joshi SV, Drzal LT, Mohanty AK, Arora S. Compos A Appl Sci Manuf 2004;35:371–6.
[8] Bourmaud A, Beaugrand J, Shah DU, Placet V, Baley C. Prog Mater Sci 2018;97:347–408.
[9] Oksman K, Skrifvars M, Selin J-F. Compos Sci Technol 2003;63:1317–24.
[10] Rueppel M, Rion J, Dransfeld C, Fischer C, Masania K. Compos Sci Technol 2017;146:1–9.
[11] Duc F, Bourban P-E, Plummer C, Månson J-A. Compos A Appl Sci Manuf 2014;64:115–23.
[12] Kabir M, Wang H, Lau K, Cardona F. Compos B Eng 2012;43:2883–92.
[13] Sachs R, Ihde J, Wilken R, Mayer B. Plasma 2019;2:272–82.
[14] Aydın M, Tozlu H, Kemaloglu S, Aytac A, Ozkoc G. J Polym Environ 2011;19:11–7.
[15] Hegemann D, Körner E, Albrecht K, Schütz U, Guimond S. Plasma Processes Polym 2010;7:889–98.
[16] Bessa J, Matos J, Mota C, Cunha F, Araújo I, Silva L, et al. Procedia Eng 2017;200:465–71.
[17] Seychal G, Perli G, Goldberg A, Sardon H, Aranburu N, Raquez J-M. Adv Compos Hybrid Mater 2025;8:426.
[18] Ng W, Johar M, Israr H, Wong K. Interfaces in Particle and Fibre Reinforced Composites 2020:163–98.
[19] Woigk W, Fuentes C, Rion J, Hegemann D, Van Vuure AW, Dransfeld C, et al. Compos A Appl Sci Manuf 2019;122:8–17.
[20] Tran LQN, Fuentes C, Dupont-Gillain C, Van Vuure AW, Verpoest I. Compos Sci Technol 2013;80:23–30.
[21] Mohanty AK, Vivekanandhan S, Pin J-M, Misra M. Science 2018;362:536–42.
[22] Park J-M, Quang ST, Hwang B-S, DeVries KL. Compos Sci Technol 2006;66:2686–99.
[23] Woigk W, Fuentes C, Rion J, Hegemann D, Van Vuure AW, Kramer E, et al. Compos Sci Technol 2019;183:107791.
[24] Fuentes C, Zhang Y, Guo H, Woigk W, Masania K, Dransfeld C, et al. Colloids Surf A Physicochem Eng Asp 2018;558:280–90.
[25] Faruk O, Bledzki AK, Fink H-P, Sain M. Prog Polym Sci 2012;37:1552–96.
[26] Baltazar-Y-Jimenez A, Bismarck A. Green Chem 2007;9:1057–66.
[27] Bozaci E, Sever K, Sarikanat M, Seki Y, Demir A, Ozdogan E, et al. Compos B Eng 2013;45:565–72.
[28] Marais S, Gouanvé F, Bonnesoeur A, Grenet J, Poncin-Epaillard F, Morvan C, et al. Compos A Appl Sci Manuf 2005;36:975–86.
[29] Tendero C, Tixier C, Tristant P, Desmaison J, Leprince P. Spectrochim Acta B At Spectrosc 2006;61:2–30.
[30] Kalia S, Kaith B, Kaur I. Polym Eng Sci 2009;49:1253–72.
[31] Mukhopadhyay S, Fangueiro R. J Thermoplast Compos Mater 2009;22:135–62.
[32] Seghini MC, Touchard F, Sarasini F, Chocinski-Arnault L, Tirillo J, Bracciale MP, et al. Cellul 2020;27:511–30.
[33] Sarikanat M, Seki Y, Sever K, Bozaci E, Demir A, Ozdogan E. J Ind Text 2016;45:1252–67.
[34] Baltazar-y-Jimenez A, Bistritz M, Schulz E, Bismarck A. Compos Sci Technol 2008;68:215–27.
[35] Seki Y, Sarikanat M, Sever K, Erden S, Ali Gulec H. Fibers Polym 2010;11:1159–64.
[36] Lapena MH, Lopes CMA. Plasma Processes Polym 2023;20:2200081.
[37] Chen F, Liu W, Zhang D. Appl Surf Sci 2023;641:158488.
[38] Moisan M, Pelletier J. *Physics of collisional plasmas: introduction to high-frequency discharges*. Springer Science & Business Media; 2012.
[39] Sun D, Stylios G. J Mater Process Technol 2006;173:172–7.
[40] Petrov G, Apruzese J, Petrova TB, Wolford M. J Appl Phys 2016:119.
[41] Zhong S, Yang B, Ou Q. Plasma Sci Technol 2015;17:767.
[42] Wielage B, Lampke T, Marx G, Nestler K, Starke D. Thermochim Acta 1999;337:169–77.
[43] Amberg M, Hanselmann B, Hegemann D. Surf Coat Technol 2025;497:131806.
[44] Pedersen JD, Teh KS. MRS Online Proceedings Library (OPL) 2011;1323:mrss11-1323-c1303-1323.
[45] She Y, Lee J, Diroll BT, Lee B, Aouadi S, Shevchenko EV, et al. ACS Omega 2017;2:7812–9.
[46] Černák M, Hudec I, Kováčik D, Zahoranová A. The European Physical Journal-Applied Physics 2009;47:22806.
[47] Černák M, Kováčik D, Ráhel' J, St'Ahel P, Zahoranová A, Kubincová J, et al. Plasma Phys Controlled Fusion 2011;53:124031.
[48] Della Volpe C, Maniglio D, Siboni S, Morra M. J Adhes Sci Technol 2003;17:1477–505.

[49] Tran LQN, Fuentes C, Dupont-Gillain C, Van Vuure AW, Verpoest I. Colloids Surf A Physicochem Eng Asp 2011;377:251–60.
[50] Fuentes C, Brughmans G, Tran L, Dupont-Gillain C, Verpoest I, Van Vuure AW. Compos Sci Technol 2015;109:40–7.
[51] Hegemann D, Janůšová M, Navascués P, Zajíčková L, Guex AG. Adv Mater Interfaces 2025;12:2400727.
[52] Bacharouche J, Kunemann P, Fioux P, Vallat M-F, Lalevée J, Hemmerlé J, et al. Appl Surf Sci 2013;270:64–76.
[53] Vandenbossche M, Hegemann D. Curr Opin Solid State Mater Sci 2018;22:26–38.
[54] Hegemann D. Thin Solid Films 2015;581:2–6.
[55] Cimerman R, Hensel K. Plasma Chem Plasma Process 2023;43:1411–33.
[56] Portugal S, Roy S, Lin J. Sci Rep 2017;7:6388.
[57] Park S, Choe W, Jo C. Chem Eng J 2018;352:1014–21.
[58] Qiu S, Wang J, Zhang D, Van Vuure AW, Seveno D, Fuentes CA. J Colloid Interface Sci 2019;557:349–56.
[59] Swolfs Y, McMeeking RM, Verpoest I, Gorbatikh L. Compos A Appl Sci Manuf 2015;69:279–87.
[60] Li L, Swolfs Y, Straumit I, Yan X, Lomov SV. J Compos Mater 2016;50:1921–35.
[61] Puck A, Schürmann H. Compos Sci Technol 1998;58:1045–67.
[62] Puck A, Deuschle HM. Compos Sci Technol 2002;62:371–8.
[63] Kolářová K, Vosmanská V, Rimpelová S, Švorčík V. Cellul 2013;20:953–61.
[64] Swolfs Y, Verpoest I, Gorbatikh L. Compos Sci Technol 2015;114:42–9.
[65] Hao J, Bardon J, Mertz G, Fuentes C, Van Vuure AW. Compos A Appl Sci Manuf 2024;185:108322.
[66] Hao J, Prapavesis A, Lomov SV, Fuentes C, Van Vuure AW. Compos Struct 2024;329:117786.
[67] Swolfs Y, McMeeking RM, Verpoest I, Gorbatikh L. Compos Sci Technol 2015;108:16–22.
[68] Hao J, Bardon J, Mertz G, Fuentes C, Van Vuure AW. Polym Compos 2025.